

# Flow-induced particle migration in microchannels for improved microfiltration processes

A. M. C. van Dinther · C. G. P. H. Schroën ·  
A. Imhof · H. M. Vollebregt · R. M. Boom

Received: 31 October 2012 / Accepted: 12 February 2013 / Published online: 1 March 2013  
© Springer-Verlag Berlin Heidelberg 2013

**Abstract** Microchannels can be used to induce migration phenomena of micron sized particles in a fluid. Separation processes, like microfiltration, could benefit from particle migration phenomena. Currently, microfiltration is designed around maximum flux, resulting in accumulation of particles in and on the membrane. In this paper it is shown that starting the design at the particle level will result in a new microfiltration process. The behaviour of suspensions between 9 and 38 volume% was studied by confocal scanning laser microscopy; migration as a result of shear-induced diffusion was observed in a rectangular microchannel with nonporous walls. Particles segregated on size within the first 10 cm of the channel. To illustrate this, at 20 volume% of small (1.53  $\mu\text{m}$ ) and large (2.65  $\mu\text{m}$ ) particles each, the larger particles migrated to the middle of the channel, while the small particles had high concentrations near the walls. The small particles could then be collected from their position close to the permeable walls, e.g. membranes, where the pore size of the membrane is no longer the determining factor for

separation. Guidelines for using this phenomenon in a microfiltration process were derived and the selectivity of the process was experimentally evaluated. The small droplets could be removed from the mixtures with a membrane having pores 3.7 times larger than the droplets, thereby minimizing accumulation of droplets in and on the membrane. As long as the process conditions are chosen appropriately, no droplet deposition takes place and high fluxes ( $1.7 \times 10^3 \text{ L h}^{-1} \text{ m}^{-2} \text{ bar}^{-1}$ ) can be maintained.

**Keywords** Shear-induced particle migration · Microchannel · Fractionation · Microfiltration · Confocal scanning laser microscopy

## List of symbols

$a$	Particle radius (m)
$b$	Fitting parameter (–)
$c$	Fitting parameter (–)
$d_L$	Diameter large emulsion droplets (m)
$d_S$	Diameter small emulsion droplets (m)
$D$	Stokes–Einstein diffusivity ( $\text{m}^2/\text{s}$ )
$D_\phi$	Dimensionless diffusion coefficient (–)
$D_{\text{shear}}$	Shear-induced diffusion coefficient ( $\text{m}^2/\text{s}$ )
$E_L$	Dimensionless evolution length (–)
$E_p$	Evolution parameter (–)
$E_p^{\text{fit}}$	Fitted evolution parameter (–)
$E_p^{\text{fit}}_{\text{norm}}$	Normalized fitted evolution parameter (–)
$H$	Half the channel height (m)
$k$	Boltzmann constant (J/K)
$K$	Constant related to shear-induced diffusion (–)
$L$	Channel length (m)
$Pe$	Dimensionless Péclet number relating diffusive to convective processes (–)
$Pe_{\text{Brown}}$	Dimensionless Péclet number relating Brownian to hydrodynamic forces (–)

A. M. C. van Dinther · C. G. P. H. Schroën (✉) ·  
H. M. Vollebregt · R. M. Boom  
Food Process Engineering Laboratory,  
Department of Agrotechnology and Food Sciences,  
Wageningen University, Bomenweg 2,  
6703 HD Wageningen, The Netherlands  
e-mail: Karin.Schroen@wur.nl

A. Imhof  
Soft Condensed Matter, Debye Institute for Nanomaterials  
Science, Utrecht University, Princetonplein 5,  
3584 CC Utrecht, The Netherlands

H. M. Vollebregt  
Wageningen UR Food and Biobased Research,  
Bornse Weilanden 9, 6708 WG Wageningen,  
The Netherlands

$Pe_{\text{shear}}$	Dimensionless Péclet number relating shear-induced diffusive to hydrodynamic forces (–)
$Re_c$	Dimensionless channel Reynolds number (–)
$Re_p$	Dimensionless particle Reynolds number (–)
$t$	Time (s)
$T$	Temperature (K)
$\bar{v}$	Average velocity (m/s)
$w$	Channel width (m)
$x$	Distance in the channel parallel to the flow (m)
$X$	Dimensionless distance from the inlet (–)
$y$	Average distance travelled by the particles perpendicular to the flow (m)
$z$	Position of particle relative to reference wall (m)

### Greek symbols

$\alpha$	Selectivity of membrane process (–)
$\dot{\gamma}$	Shear rate (1/s)
$\eta$	Viscosity of the solution (Pa s)
$\eta(\varphi)$	Viscosity as a function of the solid volume fraction of the suspension (Pa·s)
$\lambda$	Constant related to shear-induced diffusion (–)
$\rho$	Density of the suspension (kg/m <sup>3</sup> )
$\rho_{\text{oil}}$	Density of the oil phase (kg/m <sup>3</sup> )
$\tau_{\text{con}}$	Time scale of convection (s)
$\tau_{\text{dif}}$	Time scale for migration (s)
$\varphi$	Solid volume fraction of the suspension (–)
$\varphi_L$	Solid volume fraction of large particles (–)
$\varphi_{L,b}$	Solid volume fraction of the large particles in the bulk (–)
$\varphi_{L,p}$	Solid volume fraction of the large particles in the permeate (–)
$\varphi_S$	Solid volume fraction of small particles (–)
$\varphi_{S,b}$	Solid volume fraction of the small particles in the bulk (–)
$\varphi_{S,p}$	Solid volume fraction of the small particles in the permeate (–)
$\varphi_{\text{tot}}$	Solid volume fraction of the bidisperse suspension (–)
$\varphi(x, z)$	Concentration profile of particles at a certain distance in the channel (–)
$\varphi_{\text{ref}}(z)$	Concentration profile at the inlet (–)
$\langle \varphi(x, z) \rangle_z$	Cross-sectional average volume fraction (–)
$\langle \varphi_{\text{ref}}(z) \rangle_z$	Cross-sectional average volume fraction at the inlet (–)

## 1 Introduction

Microfluidic devices are increasingly used in, for example, (cell) biology, food, pharmaceuticals and chemical synthesis (Whitesides 2006). Their advantages are the small volume and large surface area, leading to better mass and heat transfer. Besides, they can be used to manipulate not only

multiphase systems (e.g. for the preparation of droplets or particles) but also particle suspensions or emulsions and induce migration phenomena. This last aspect of microfluidic devices can be applied to separation processes to improve their performance. Several articles describe the potential of microfluidic devices for separation purposes (Lenshof and Laurell 2010; Weigl and Yager 1999; Bhagat et al. 2010; Zhao and Cheng 2011; Bhagat et al. 2009; Di Carlo 2009; Pamme 2007). In this article we show how the use of microchannels in a microfiltration set-up can tackle current challenges in membrane microfiltration processes and can open new routes for filtration of very concentrated suspensions and emulsions, currently not possible.

Microfiltration is mostly used to remove particles from a liquid stream, for example to remove bacteria from liquid foods. It is carried out in many industries and for different applications (Strathmann 2001) and optimised for high trans-membrane flux. Membrane fouling and flux reduction as a result of (temporary) particle accumulation are then mostly taken for granted. As a result, techniques like high frequency back-pulsing may be used to temporarily remove the particles from the membrane and keep the membrane flux at acceptable levels. As the design of such processes mostly revolves around obtaining as much permeate as possible, neglecting the dynamics of the suspension on the particle level leads to fouling and therefore stresses the importance to use particle behaviour as an alternative design parameter.

When starting from the behaviour of the particle themselves, a different process that operates without fouling or flux reduction may be the result, and this could revolutionise membrane process design. The pioneering work of Belfort who described the effect of inertial lift is exemplary for this (Belfort 1989); in this paper we focus on shear-induced diffusion as migratory mechanism, but we also cover other mechanisms.

For microfiltration, the influence of process conditions on particle behaviour is of eminent importance (Belfort et al. 1994). When particles can be kept away from the membrane by adjustment of the process conditions, the trans-membrane flux and retention can be constant in time, as was illustrated in a recent publication from our lab (van Dinther et al. 2011). Even though Field et al. already introduced the importance of a steady flux by introducing the critical flux (Field et al. 1995), it is of eminent importance to understand particle migration not only in the concentration polarization layer, but also in the bulk. This approach even further improves the filtration process. The new process concept presented here is different from regular practice in two ways. The first one is operation at steady high flux and retention in time (Abbasi et al. 2011; Fillaudeau and Carrere 2002; Nandi et al. 2011; Rezaei et al. 2011; El Rayess et al. 2011) and the second, more

important one, is the possibility to fractionate very concentrated emulsions and suspensions with membranes/sieves. To achieve fractionation in concentrated systems, knowledge about particle migration in the bulk should be combined with a special design of the filtration unit. Particle migration in flowing suspensions is discussed in more detail below.

A flowing fluid exerts forces on a moving particle and this may lead to migration of particles from their streamlines (Belfort et al. 1994). Particles of different sizes are affected differently, and this may ultimately lead to a segregation of particles in the bulk of the liquid flowing over the membrane, which is useful in microfiltration. When particles segregate in the liquid before approaching the membrane surface, separation and fractionation will no longer be based on membrane pore size only (van Dinther et al. 2009; Kromkamp et al. 2006). As a result the membrane pores can be much larger and accumulation of particles on the membrane surface or in the membrane pores is prevented, as long as the process conditions remain appropriate. Such process is expected to operate much more efficiently at acceptably high fluxes, without fouling, and with less need for long and aggressive cleaning.

In a flowing suspension of micron sized particles through microchannels, hydrodynamic, lift and body forces are dominant. The migration of particles is a result of the force balance on a particle and which forces are dominant depends on the process conditions, indicating that various migration phenomena may be observed during membrane filtration (Belfort et al. 1994). In the following sections we ignore body forces, by assuming hard sphere behaviour and preventing (large) density differences between particles and the surrounding fluid. By choosing the right process conditions, the effect of Brownian motion, also a body force, is negligible compared to other mechanisms. The two main particle migration effects under the conditions relevant to microfiltration are inertial lift and hydrodynamic shear-induced diffusion and these are now discussed in more detail; the actual window of operation is given in the next section.

Lift forces are induced by shear, viscosity and inertia. The shear created when fluid flows through a channel results in a lift force causing the particle to migrate towards the wall (Eckstein et al. 1977); however, at the same time the wall-induced inertial lift force directs the particles away from the wall (Zeng et al. 2005; McLaughlin 1993). As a result the particles migrate to a certain equilibrium position (Eloot et al. 2004); this is called the Segré–Silberberg effect or ‘Tubular Pinch’.

Velocity gradients can also lead to shear-induced migration of particles. Particles rotate with an angular velocity and circulatory fluid motion is established around the particle creating a velocity field that exerts drag on neighbouring particles (Piron et al. 1995). Besides this,

particles pass other particles in slower-moving fluid streamlines, thereby causing ‘collisions’ based on excluded volume, usually without contact, which causes particles to move to other streamlines (Eckstein et al. 1977). When three or more particles are involved simultaneously, the net displacement is random, resulting in a diffusion-type of behaviour of the particles.

Phillips et al. (1992) estimated the total flux due to shear-induced diffusion in a straight channel with Eq. 1:

$$J = -D_{\text{shear}} \nabla \left( \ln \left( \dot{\gamma} \varphi \eta^\lambda \right) \right) \quad (1)$$

In which

$$D_{\text{shear}} = K \dot{\gamma} a^2 \varphi^2 \quad (2)$$

With  $a$  the particle radius (m),  $\varphi$  the solid volume fraction (–),  $\dot{\gamma}$  the shear rate (1/s),  $\eta$  the viscosity (Pa s),  $\lambda$  a constant (–),  $D_{\text{shear}}$  the shear-induced diffusion coefficient (m<sup>2</sup>/s) and  $K$  a constant (–) that may be dependent on the volume fraction (Leighton and Acrivos 1987a, b). Gradients in shear rate, concentration and in viscosity all give rise to migration.

The migration thus depends on particle radius (via  $D_{\text{shear}}$ ) and concentration (via the driving forces and  $D_{\text{shear}}$ ) and it is therefore clear that particles with different sizes and concentrations will have different migration velocities. Larger particles interact more easily with streamlines of neighbouring particles due to their size and thereby easily move to other streamlines, leading to faster migration (Eloot et al. 2004). As a result, larger particles will concentrate towards the middle of the channel while smaller particles are in the region close to the wall (Leighton and Acrivos 1987b; Breedveld et al. 2001; Tan 2003; Graham et al. 1991; Lyon and Leal 1998a, b).

One may also make good use of this segregation in microchannels as is done in this paper. Shear-induced diffusion is especially dominant in concentrated suspensions, which easily lead to fouling in and on the membrane during regular microfiltration, due to the large amount of particles present. In this paper, this shear-induced diffusion of particles is shown to be dominant in concentrated suspensions flowing through microchannels and can be used to enhance membrane processes.

Although research has been done on migration phenomena in channels with nonporous walls and Couette devices (Abbott et al. 1991; Acrivos et al. 1993; Chow et al. 1994; Graham et al. 1991; Shakib-Manesh et al. 2002; Tetlow et al. 1998; Yu et al. 2007), as well as on particle migration in membrane microfiltration (Vollebregt et al. 2010; Belfort et al. 1994; Belfort 1989; Kromkamp 2005), it has never been investigated how particle migration in a microchannel with nonporous walls may be utilised for microfiltration. In other words, how particle migration in

concentrated suspensions can be used to make fractionation of particles possible with an energy-efficient process like microfiltration.

Semwogerere et al. (Semwogerere et al. 2007; Semwogerere and Weeks 2008) summarized the influence of the ratio of particle sizes on the development of the concentration profile. The development of the concentration profile was captured into an evolution parameter. From this parameter, the evolution length can be calculated, which is related to the point where the concentration profile is completely developed. Even though also partially developed profiles show segregation, this evolution length may be used as a guideline to identify process conditions and module designs of interest.

In this paper, concentration profiles are experimentally determined by confocal scanning laser microscopy (CSLM) in bi-disperse suspensions flowing in microchannels with nonporous walls. Insights in the most important process parameters for particle migration and segregation of particles on size in fluid flow are obtained, giving guidelines to use shear-induced migration for fractionation in new separation processes. At the end of the experimental section, a proof of principle is shown in which a membrane process is designed around these new insights.

### 1.1 Window of operation

The degree of migration can be estimated by investigating the balance between the time scales of the convection through the tube or channel and the particle migration mechanisms perpendicular to the main flow direction (Nott and Brady 1994). The shear rate is related to the flow velocity. In Eq. 3 one can see the relation for Poiseuille flow:

$$\dot{\gamma} = \frac{3\bar{v}}{H} \quad (3)$$

where  $\bar{v}$  is the average velocity (m/s) and  $H$  is half the channel height (m). We only consider a laminar regime here, since turbulence would disturb particle migration. The time scale of convection  $\tau_{\text{con}}$  (s) is given by Eq. 4.

$$\tau_{\text{con}} = \frac{L}{\bar{v}} = \frac{3L}{\dot{\gamma}H} \quad (4)$$

where  $L$  is the channel length (m).

The time scale of the migration mechanisms depends on the average distance travelled by the particles perpendicular to the flow. The average distance travelled by the particles perpendicular to the flow ( $y$  (m)) is described in Eq. 5.

$$y = 2(Dt)^{\frac{1}{2}} \quad (5)$$

with  $t$  the time (s) and  $D$  the diffusivity. The diffusivity may incorporate several migration mechanisms

(Vollebregt et al. 2010) of which the two most important ones for the experimental set-up are described below. The channel half-height ( $H$ ) can be seen as measure for the distance that the particles have to travel.

This leads to the time scale for migration ( $\tau_{\text{dif}}$ (s)), defined in Eq. 6.

$$\tau_{\text{dif}} = \frac{H^2}{4D} \quad (6)$$

The ratio between the time scales is a Péclet number defining the ratio of diffusive and convective processes (Eq. 7). The Péclet number is different for different migration mechanisms.

$$\text{Pe} = \frac{\tau_{\text{dif}}}{\tau_{\text{con}}} = \dot{\gamma} H^2 \frac{1}{12d} \frac{H}{L} \quad (7)$$

### 1.2 Brownian motion

Brownian motion is a body force which leads to random motion of particles. The Péclet number gives the relative importance of Brownian to hydrodynamic forces (Ackerson 1991); at a Péclet number  $>1$ , the hydrodynamic forces dominate Brownian motion. Brownian motion is only visible at small scales and therefore the half-channel height is not a good measure for the average distance travelled by the particles. The migration is more likely to be dominant at the particle level and therefore the particle radius is chosen as a more reliable length scale. Simplified, the Péclet number is therefore defined as in Eq. 8.

$$\text{Pe}_{\text{Brown}} = \frac{\dot{\gamma} \alpha^2}{D} \quad (8)$$

In which  $D$  is defined by the Stokes–Einstein diffusivity ( $\text{m}^2/\text{s}$ ) given in Eq. 9.

$$D = \frac{kT}{6\pi\eta a} \quad (9)$$

where  $k$  is the Boltzmann constant ( $1.380 \times 10^{-23}$  J/K),  $T$  is the temperature (K), and  $\eta$  is the viscosity of the suspension (Pa s).

From Eq. 8, the minimal shear rate needed to circumvent the influence of Brownian diffusion is derived and subsequently we can derive the minimal velocity ( $v_{\text{min}}$ ) by using Eq. 3. For dimensionless channel lengths (length in the channel divided by half its height) of 2,400 and 4,800, the minimum velocity is 3.30 and 0.63  $\mu\text{m}/\text{s}$ , for 1.53 and 2.65  $\mu\text{m}$  diameter particles, respectively ( $\text{Pe}_{\text{Brown}} > 1$ ). In all the experiments the velocity is larger than  $v_{\text{min}}$ , indicating that Brownian diffusion of suspension particles is not important. The average shear rate is used in the calculations and Brownian motion plays a role in the middle of the channel where the shear rate is zero or close to zero. This will result in the random motion of particles and

reduces the shear-induced diffusion in this region of the channel. Further away from the centre this situation changes quickly, where the average velocity is much higher than the minimum velocity required to circumvent the influence of Brownian diffusion (8.3 and 20.8 μm/s).

Important aspects in particle migration and applications like microfiltration are pH and temperature. Brownian motion is influenced by temperature (Eq. 9). Particle size can also be influenced by temperature and pH, leading to a change in Péclet number (both for Brownian motion and shear-induced diffusion). Besides, additional repulsion or attraction of particles could play a role at different pH and temperature, but these aspects are considered beyond the scope of this paper.

### 1.3 Shear-induced migration

Shear-induced diffusion is dominant in concentrated suspensions, and if fractionation is aimed for, particles should have sufficient time to migrate. A short distance to travel, i.e. a low channel height which is the case in microchannels, leads to faster migration. This means that the time scale for migration, i.e. shear-induced diffusion, should be smaller than that for convection, and this can be related to an evolution length for the CSLM experiments (Nott and Brady 1994).

In Eq. 6, the diffusivity is described by  $D_{\text{shear}}$  defined as  $D_{\text{shear}} = \dot{\gamma} a^2 D_\phi$  (Leighton and Acrivos 1987b).  $D_\phi$  is the dimensionless diffusion coefficient defined in Eq. 10.

$$D_\phi = \frac{1}{3} \phi^2 (1 + 0.5e^{8.8\phi}) \tag{10}$$

The evolution length (see respective section) is defined as the length at which the particles have migrated a pre-set distance, in our case half the channel height. It must be noted that estimates based on this are conservative; not all particles have to travel half the channel height. In a membrane process the large particles would need to move thus far that they are not incorporated in the permeate, while the small ones can stay close to the walls. The Péclet number defined in Eq. 7 therefore becomes as described in Eq. 11.

$$\text{Pe}_{\text{shear}} = \frac{\tau_{\text{dif}}}{\tau_{\text{con}}} = \left(\frac{H}{a}\right)^2 \frac{1}{12D_\phi} \frac{H}{L} \tag{11}$$

### 1.4 Evolution length

The evolution length is the channel length necessary to establish migration patterns and it can be calculated for different degrees of migration (fully or partially developed). For membrane microfiltration, migration of particles should occur, but the concentration profile does not have to be complete as mentioned before. Additionally, if a

channel with nonporous walls is used prior to a channel with porous wall, the total length of the module should be kept as short as possible, to prevent unacceptable pressure drops, being in the order of millibars for the experiments.

The size and concentration distribution at different positions in the channel was analysed with confocal scanning laser microscopy (CSLM). The evolution length, i.e. length at which the concentration profile is completely developed, could be evaluated from the so-called evolution parameter ( $E_p(x)$ ), introduced by Semwogerere et al. (Semwogerere et al. 2007; Semwogerere and Weeks 2008). This parameter determines the degree of development of the concentration profile (with particles) and is described in Eq. 12.

$$E_p(x) = \frac{1}{2H} \int_0^{2H} \left| \frac{\varphi(x, z)}{\langle \varphi(x, z) \rangle_z} - \frac{\varphi_{\text{ref}}(z)}{\langle \varphi_{\text{ref}}(z) \rangle_z} \right| dz \tag{12}$$

In the equation  $\varphi(x, z)$  is the concentration profile of particles at a certain distance in the channel (–),  $\varphi_{\text{ref}}(z)$  is the concentration profile at the inlet (–),  $\langle \varphi(x, z) \rangle_z$  is the cross-sectional average volume fraction (–) and  $\langle \varphi_{\text{ref}}(z) \rangle_z$  is the cross-sectional average volume fraction at the inlet (–).

The evolution parameter is fitted with an exponential function (Eq. 13), for which a simplified fit with two variables was used.

$$E_p^{\text{fit}}(X) = b(1 - e^{-cX}) \tag{13}$$

$X$  is the dimensionless distance from the inlet and defined as  $x/H$  (–),  $b$  and  $c$  are fitting parameters, with  $c$  defined as  $E_L^{-1}$  [ $E_L$  is the dimensionless evolution length (–)]. The fit is normalized using the value for  $b$  (Eq. 14), after which the curves can be compared directly.

$$E_p^{\text{fit}}_{\text{norm}}(X) = E_p^{\text{fit}}(X)/b \tag{14}$$

### 1.5 Inertial lift

Inertial lift is exerted on a particle by the fluid, due to the flow profile and the proximity of wall. It is dependent on the particle Reynolds number, as given by Eq. 15, which in turn is a function of the channel Reynolds number (Eq. 16) (Park et al. 2009). Whether inertial lift plays a role depends on the ratio between inertial and viscous forces; generally at particle Reynolds numbers  $>1$  (Asmolov 1999), inertial lift is relevant. In all experiments the particle Reynolds numbers were below  $9 \times 10^{-7}$ , indicating that inertial lift did not play a role.

$$\text{Re}_p = \text{Re} \left( \frac{2a(w + 2H)}{4wH} \right)^2 = \frac{\gamma a^2 \rho (w + 2H)}{3\eta_\phi w} \tag{15}$$

with

$$\text{Re}_c = \left( \frac{4wH}{(w + 2H)} \right) \frac{\bar{v}\rho}{\eta_\phi} \quad (16)$$

where  $\text{Re}_c$  is the channel Reynolds number defined in Eq. 16,  $\rho$  is the density of the suspension ( $\text{kg/m}^3$ ),  $w$  is the channel width (m) and  $\eta_\phi$  is the viscosity as a function of the solid volume fraction of the suspension (Pa s).

## 2 Experimental

### 2.1 Particle migration in channel with nonporous walls

The experiments were carried out with a confocal scanning laser microscope (Leica SP2, Germany), with a  $63 \times 1.4$  numerical aperture oil immersion objective and laser light with a wavelength of 543 and 488 nm. The height of the focal plane could be positioned with a piezo-focusing drive (P-721, Physik Instrumente, Germany).

Two types of PMMA (polymethyl methacrylate) particles were made by dispersion polymerization and fluorescently labelled with NBD (7-nitrobenzo-2-oxa-1,3-diazole) and rhodamine B fluorescent dye, respectively (Bosma et al. 2002). The smallest particles had an average diameter of  $1.53 \mu\text{m}$  and the larger ones a diameter of  $2.65 \mu\text{m}$ . The polydispersity of the particles was 2.5 %. The particles were dispersed in a mixture of 72.8 % cyclohexylbromide and 27.2 % cis-decalin to match the refractive indices of particles and surrounding liquid. The solvent was saturated with tetrabutylammoniumbromide (TBAB) to screen any small particle charges, and make them behave like hard spheres. Stock suspensions were mixed in the desired ratio, and pumped through a glass rectangular channel with a syringe pump (Pico Plus, Harvard Apparatus, USA). The channel was 30 cm by 2 mm by  $100 \mu\text{m}$  (length, width, height, respectively) (Friedrich and Dimmock Inc., USA). A holder was constructed in order to prevent the glass channel from breaking and to make the connection to the syringe (Fine-mechanical workshop, Wageningen University). For the velocities investigated in our experiments we only need  $2H$  length to establish a fully developed fluid velocity profile (Shah and London 1978) (please note that this does not coincided with the particle concentration profile), and therefore the 0.3 m long channel with

nonporous walls was more than long enough; also the membrane module satisfies this prerequisite.

The pictures taken (at 12 and 24 cm from the entrance of the channel) consisted of 512 by 64 pixels, corresponding to a field of view of  $59.52$  by  $7.44 \mu\text{m}$  with a depth of  $\sim 250 \text{ nm}$ . The system was operated in the xyt-mode, with a zoom of 4 and a scanning frequency 400 Hz. Here,  $x$  is oriented along the channel length and  $y$  along the width. The frame rate used was 10 frames/s. Under these circumstances velocities up to  $590 \mu\text{m/s}$  can be measured; experimental velocities are always lower. The pictures were analysed with the image processing toolbox in MATLAB (Mathworks, US) to determine particle number, type and velocity. The experimental set-up is shown in Fig. 1.

From Eqs. 10 and 11 in the former section, the minimal solid volume fraction ( $\phi_{\text{min}}$ ) for migration for shear-induced diffusion to be relevant ( $\text{Pe}_{\text{shear}} < 1$ ) can be derived and the results are presented in Table 1. For these data, it is assumed that the dimensionless diffusion coefficient is given by the relation derived by Leighton and Acrivos (Eq. 10) (Leighton and Acrivos 1987b). These values are valid for a monodisperse suspension, where the Péclet number is determined on the basis of the total volume fraction of the suspension. From this it can be concluded that  $1.53 \mu\text{m}$  particles are expected to show significant migration behaviour at total solid volume fraction  $>0.23$  at a given channel length. For the  $2.65 \mu\text{m}$  particles, migration is expected at volume fractions  $>0.16$ . For fractionation purposes, migration of the small particles to the middle is not preferred and in the experiments the solid volume fractions of the small particles does not exceed 0.19. The solid volume fractions of the large particles range from 0.09 to 0.36.

### 2.2 Membrane microfiltration

For the membrane microfiltration experiments a nickel membrane with spherical pores of  $20 \mu\text{m}$  was used to fractionate the emulsions (Veconic sieve, Stork Veco BV, the Netherlands). The membrane was placed in a module with a length of 40.5 cm, of which the first 34.5 cm was a channel with nonporous walls to establish a fully developed velocity profile. Within this length, the concentration profiles are also well established, concluded based on the

**Fig. 1** Schematic drawing of the experimental set-up for the particle migration in channel with nonporous walls

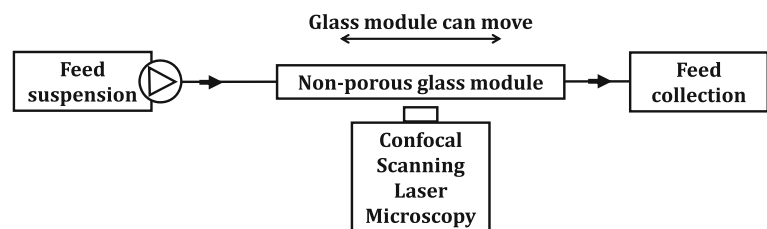


**Table 1** Minimal solid volume fraction for migration of 1.53 and 2.65  $\mu\text{m}$  diameter particles as a function of dimensionless length in the rectangular channel

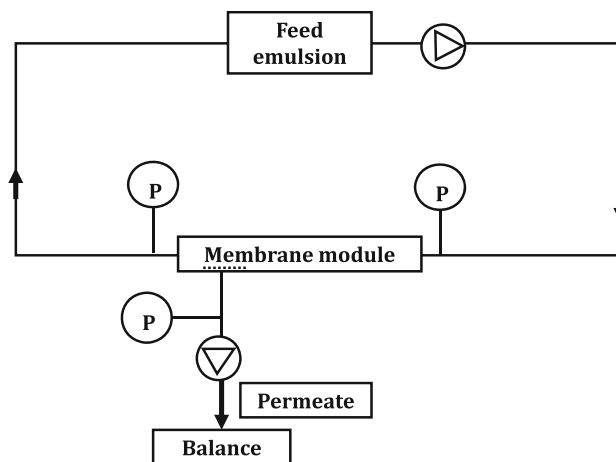
	1.53 $\mu\text{m}$ particles	2.65 $\mu\text{m}$ particles
$L/H$ (–)	$\varphi_{\text{min}}$ (–)	$\varphi_{\text{min}}$ (–)
2,400	0.27	0.20
4,800	0.23	0.16

calculated evolution lengths (Sect. 3). In hollow fibre membrane filtration, the potting area where no flux is possible can be used for this purpose, if the membranes have the same pore size as used in this paper and the channel/fibre diameter is similar. In our experiments we used a membrane, which was placed after 34.5 cm and had an area of 1.39  $\text{cm}^2$ . The height of the channel could be changed, but was kept at its minimum of 200  $\mu\text{m}$ . The emulsion was fed to the system with a positive displacement pump (VG1000digit, Verdergear, Germany).

Pressure sensors (EL-PRESS P-502C, Bronkhorst High-Tech B.V., The Netherlands) were installed at the beginning and the end of the module, and after the membrane. The pressure data were recorded with Bronkhorst High-Tech software. The trans-membrane pressure is much lower than normally applied in microfiltration with values around 10–30 mbar. The transmembrane flux was measured with a balance (CP4202S, Sartorius, Germany) connected to a computer (Memfill-Lite software, Wageningen University, the Netherlands). The permeate flow was set at a specific value with a peristaltic pump (series 205U, Watson Marlow, England). The measured flux and pressures were constant in time, which indicates no accumulation of particles on/in the membrane. The membrane flux was checked before and after filtration for cracks/production errors and fouling. The membrane is a metallic sieve and therefore neither very vulnerable to cracks nor to fouling, also because the process is operated in such a way that the droplets move away from the surface and the pores are much larger than the largest droplets. The experimental set-up is shown in Fig. 2.

Membrane microfiltration experiments were performed with two emulsions that were mixed in a pre-determined ratio; the oil phase consisted of silicone oil with a density of 1.01  $\text{g}/\text{cm}^3$  (silicone oil AR 20, Sigma-Aldrich, Germany). In the experiments, two oil volume fractions of 0.27 and 0.36 were used, both consisting of mixtures of two individually prepared emulsions.

For the 0.36 solid volume fraction emulsion, 36 % (w/w) silicone oil, was added to 62 % (w/w) water and 1 % (w/w) span80 (Sigma-Aldrich, Germany) as well as 1 % (w/w) Tween80 (Sigma-Aldrich, USA). A pressure vessel was filled with the mixture, which was then pressed six times through a 5  $\mu\text{m}$  filter (PVDF Durapore, Millipore

**Fig. 2** Schematic drawing of the experimental set-up for the membrane microfiltration experiment

Corporation, Bedford, USA) at 0.5 bar, which resulted in a droplet diameter of 5.1  $\mu\text{m}$  (emulsion 1). This emulsion was further refined by pressing it six times through a 2.7  $\mu\text{m}$  filter under 2 bars (Glass microfiber GD/X, Whatman, GE, USA). The typical diameter of this emulsion was 2.4  $\mu\text{m}$  (emulsion 2); for the separation experiments emulsions 1 and 2 were mixed at set ratios.

The emulsion with a solid volume fraction of 0.27, was prepared with 24 % (w/w) silicone oil, was added to 74 % (w/w) water and 1 % (w/w) span80 (Sigma-Aldrich, Germany) as well as 1 % (w/w) Tween80 (Sigma-Aldrich, USA). Again two emulsions were made, similar to the procedure described above. The typical diameter of the first emulsion was 2.4  $\mu\text{m}$ , while the second had a diameter of 5.4  $\mu\text{m}$ .

Droplet sizes of initial emulsions, mixtures and permeate were measured in the Malvern Mastersizer (Malvern Instruments Ltd, UK). The total amount of oil droplets was determined by a dry weight measurement, for which the samples were stored overnight in an oven at 80  $^{\circ}\text{C}$  (Mettler, Germany). The ratio between large and small droplets was determined by analysis of the Malvern Mastersizer data. The experiments were run for 15 min to stabilize. Samples were taken after 15, 30 and 45 min and analysis results were stable in time.

### 3 Results

For the investigated process conditions, shear-induced diffusion was the dominant particle migration mechanism and neither inertial lift nor Brownian diffusion was expected to influence the results as described in Sect. 1.1. From the calculated evolution lengths (Eqs. 12 and 13), we concluded that the concentration profiles under all conditions are well established within our module length.

The concentration profile develops very fast within the first 0.1 m of the module, which implies that in membrane microfiltration only 0.1 m of non-porous channel is needed to allow for sufficient particle migration to take place. In this section, the results obtained with the CSLM will be described followed by an evaluation of the options for membrane separation, being experimentally determined afterwards.

### 3.1 Confocal scanning laser microscopy in microchannel with nonporous walls

The results are shown at different positions in the microchannel with nonporous walls expressed as  $x/H$ , the distance  $x$  relative to the entrance of the channel over half-channel height  $H$ . This distance was 12 and 24 cm from the entrance length and therefore longer than the first 10 cm in which the concentration profile develops drastically. On the horizontal axis of the graphs, the dimensionless height  $z/2H$  is used, with  $z$  the position of the particle relative to the reference wall (m). Further, the total particle fraction  $\varphi_{\text{tot}}$  and the fraction of small particles  $\varphi_s$  are indicated.

The concentration profiles of large and small particles develop in the channel, and a striking example can be seen in Fig. 3. Large particles are migrating to the middle, while small particles have higher concentrations near the wall, and this ‘pre-fractionation’ of particles in the liquid will later be used to facilitate particle separation. The effect is caused by shear-induced diffusion that causes particles to migrate away from the walls. Larger particles experience a much stronger driving force, probably displacing the smaller ones to the walls.

In the next sections, the influence of process conditions on the concentration profiles of the two particles’ sizes is described. Subsequently, guidelines for membrane microfiltration processes are extracted.

#### 3.1.1 Velocity

Two flow velocities, 8.3 and 20.8  $\mu\text{m/s}$ , were used at a total volume fraction of 0.19. The solid volume fraction of small particles relative to the total solid volume fraction was 0.1 and 0.5 (with total solid volume fraction  $\varphi_s$  0.02 and 0.09) (Fig. 4a, b). For both cases, no difference in concentration profile of the large particles was seen for the two different velocities, as was expected. The velocity, and therewith, the shear rate, is not in the Péclet number (Eq. 11), which implies that shear-induced diffusion and convection change in similar fashion. The concentration profile will only change when the velocity is below a minimum velocity related to Brownian diffusion (Table 1) or a maximum velocity that induces inertial lift. The measurement system

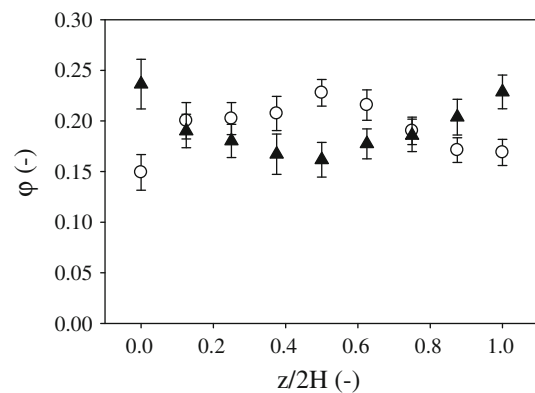


**Fig. 3** Concentration profile for 2.65  $\mu\text{m}$  (open triangle) and 1.53  $\mu\text{m}$  (closed triangle) particles.  $\varphi_{\text{tot}}$  is 0.38,  $x/H$  is 4,800,  $v$  is 20.8  $\mu\text{m/s}$  and  $\varphi_s$  is 0.19

was considered suitable to investigate shear-induced diffusion effects.

#### 3.1.2 Total solid volume fraction

The influence of the total solid volume fraction on migration behaviour is expected to be strong (Eq. 2). In Fig. 5, the concentration profiles are shown for 0.38, 0.19 and 0.09 total volume fraction, and a relative fraction of small particles of 0.04. From Fig. 5 it is clear that higher concentrations lead to steeper profiles caused by increased migration. For a low concentration of 0.09, the concentration profile is relatively flat, and it develops further with increasing concentration, with the highest concentrations in the middle of the channel.

#### 3.1.3 Relative solid volume fraction of 1.53 $\mu\text{m}$ particles

The concentration profile of the large particles is influenced by the presence of small particles. In Fig. 6, the profiles are shown for total volume fractions of 0.38, and relative solid volume fractions of small particles equal to 0.50 and 0.04 (absolute volume fraction of small particles is thus 0.19 and 0.02, respectively). The concentration profile of the large particles is more pronounced when the fraction of small particles is lower and can be related to two effects. Firstly, the large particles are known to be hindered in their movements due to the presence of small particles, therefore the black triangles in Fig. 6 have lower values at  $z/2H$  is 0.5. At the same time, the relative fraction of large particles is also higher for  $\varphi_s/\varphi_{\text{tot}}$  is 0.04 than for  $\varphi_s/\varphi_{\text{tot}}$  is 0.50, resulting in higher shear-induced diffusivity. The absolute solid volume fraction of large particles is 0.19 and 0.36, respectively. When the solid volume fraction of large particles exceeds a certain value (dependent on total concentration and fraction of small particles), shear-induced

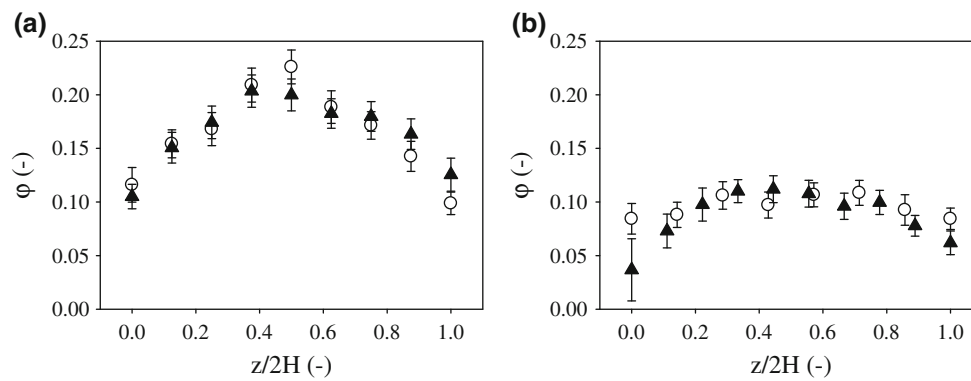


**Fig. 4** **a** Influence of velocity on concentration profile of 2.65  $\mu\text{m}$  particles. Velocities 8.3  $\mu\text{m/s}$  (open triangle) and 20.8  $\mu\text{m/s}$  (closed triangle) for  $x/H$  is 4,800,  $\varphi_s/\varphi_{tot}$  is 0.10,  $\varphi_{tot}$  is 0.19. **b** Influence of

velocity on concentration profile of 2.65  $\mu\text{m}$  particles. Velocities 8.3  $\mu\text{m/s}$  (open triangle) and 20.8  $\mu\text{m/s}$  (closed triangle) for  $x/H$  is 2,400,  $\varphi_s/\varphi_{tot}$  is 0.50,  $\varphi_{tot}$  is 0.19

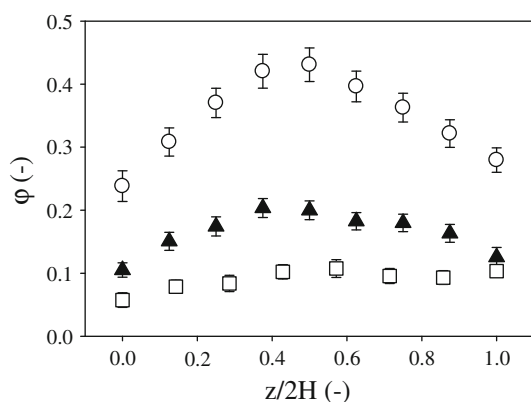


**Fig. 5** Influence of total concentration on concentration profile for 2.65  $\mu\text{m}$  particles.  $\varphi_{tot}$  is 0.38 (open triangle), 0.19 (closed triangle) and 0.09 (open square) for  $x/H$  is 4,800,  $v$  is 20.8  $\mu\text{m/s}$  and  $\varphi_s/\varphi_{tot}$  is 0.04

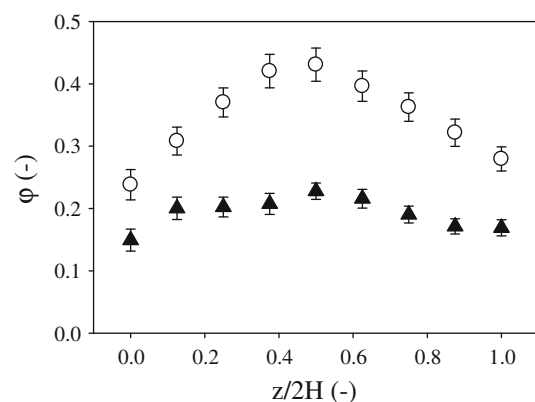


**Fig. 6** Influence of relative volume fraction of small particles [0.50 (closed triangle) and 0.04 (open triangle)] on concentration profile of 2.65  $\mu\text{m}$  particles,  $x/H$  is 4,800,  $v$  is 20.8  $\mu\text{m/s}$  and  $\varphi_{tot}$  is 0.38

diffusivity is totally determined by the large particles (Lyon and Leal 1998b).

### 3.1.4 Migration of small particles

Large particles primarily accumulated in the middle of the channel and this effect is only beneficial for separation if the profile of the small particles develops differently. Migration of large particles to the middle is preferred since large particles are more difficult to remove from smaller ones than vice versa, and at the same time, small particles should move towards the wall.

For a solid volume fraction of small particles equal to 0.19 ( $\varphi_s/\varphi_{tot}$  equal to 0.50) (Fig. 7a), the small particles have a tendency to migrate towards the wall for both velocities investigated (8.3 and 20.6  $\mu\text{m/s}$ ). The opposite occurred when the solid volume fraction of small particles was equal to 0.02 ( $\varphi_s/\varphi_{tot}$  is 0.04) (Fig. 7b), while also the large particles did not show a distinct concentration profile under the circumstances where  $\varphi_s/\varphi_{tot}$  is equal to 0.50, as

shown in Fig. 6. Most probably small particles are really migrating towards the middle instead of being excluded from the centre by large particles. Please note that the standard deviations in Fig. 7b are relatively large, due to the small amount of small particles present.

When the solid volume fraction of small particles is 0.09 ( $\varphi_s/\varphi_{tot}$  is 0.50) (as shown in Fig. 8), no particle migration was observed. The results show that for fractionation purposes, the solid volume fraction of the suspension is preferably high (e.g. 38 %), with equal solid volume fractions of small and large particles. Under these circumstances large particles migrate to the middle of the channel, while small particles are present in higher concentrations at the wall. Also Lyon and Leal (1998b) described that the solid volume fraction of the small particles should be around 0.20 to deliver a non-uniform concentration profile. Even though migration of large particles is more pronounced at smaller relative volume fractions of small particles, the selectivity of the process will be lower as a result of the simultaneous migration of small particles to the middle. Based on our

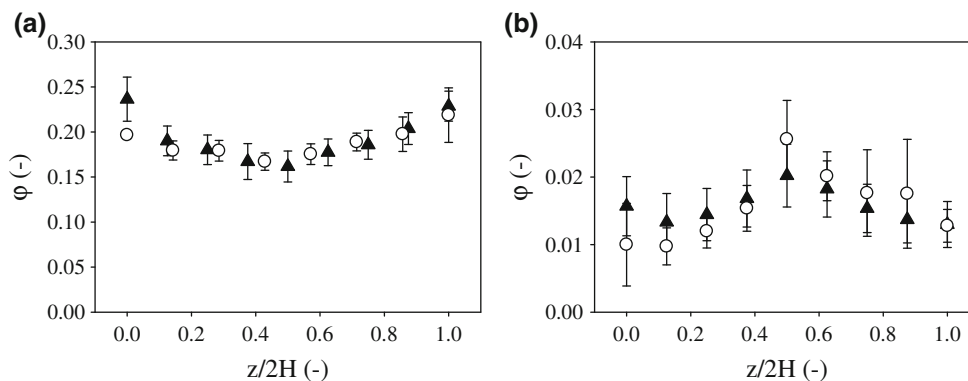


**Fig. 7 a** Concentration profile of 1.53 μm particles. Velocities 8.3 μm/s (*open triangle*) and 20.8 μm/s (*closed triangle*) for  $\phi_{tot}$  is 0.38,  $\phi_s/\phi_{tot}$  is 0.50 and  $x/H$  is 4,800. **b** Concentration profile of

1.53 μm particles. Velocities 8.3 μm/s (*open triangle*) and 20.8 μm/s (*closed triangle*) for  $\phi_{tot}$  is 0.38,  $\phi_s/\phi_{tot}$  is 0.04 and  $x/H$  is 4,800

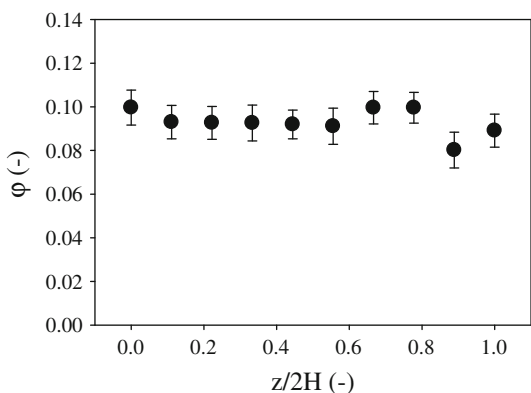


**Fig. 8** Concentration profile of 1.53 μm particles at velocity of 8.3 μm/s,  $\phi_{tot}$  is 0.19,  $x/H$  is 2,400 and  $\phi_s/\phi_{tot}$  is 0.50

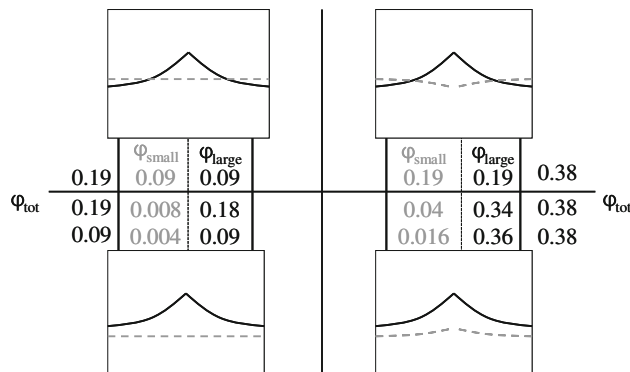


**Fig. 9** Schematic overview of concentration profiles of small (*grey, dashed lines*) and large (*black lines*) particles for different conditions; interpretation of the *graphs* is given in the last part of Sect. 3.1

results, equal solid volume fractions of large and small particles in combination with high total concentrations (e.g. 38 %; Figs. 6, 7a) are most suited for fractionation purposes.

A summary of the conditions and particle behaviour of the small and large particles is shown in the schematic overview in Fig. 9. For concentrations of 38 % (top right graph) and equal solid volume fractions of small and large particles the large particles migrate to the middle, while the small ones are mainly present at the sides. The migration of the large ones is hindered by the presence of the small ones and therefore more entrance length is needed for the profile to develop, which is not shown in the figure. As soon as the relative solid volume fraction of the small ones decreases (bottom right Figure), they migrate to the middle of the channel, although this effect is rather small. At lower concentration of particles (0.09 or 0.19; as depicted on the left of the figure) the small particles show a flat concentration profile irrespective of the volume fraction at which they are present (0.004 up to 0.09), while migration of large particles was always seen.

### 3.2 Predictions for membrane microfiltration

In this section, CSLM results are translated into predictions for membrane filtration. The measured concentration profiles are taken as a starting point, from which a certain amount of the liquid is taken out through pores at fixed positions in the wall (membrane). Permeate is taken from the liquid close to the walls of the channel and the process is operated at a flux of  $1.0 \times 10^{-5} \text{ m}^3 \text{ m}^{-2} \text{ s}^{-1}$ , which corresponds to membrane fluxes of  $4.4 \times 10^4 \text{ L h}^{-1} \text{ m}^{-2} \text{ bar}^{-1}$  (see appendix for detailed information on process conditions), due to the large pores in the membrane. Typical industrial fluxes are  $150 \text{ L h}^{-1} \text{ m}^{-2} \text{ bar}^{-1}$  with a maximum of  $2,000 \text{ L h}^{-1} \text{ m}^{-2} \text{ bar}^{-1}$  for short periods of time (Moraru and Ulrich Schrader 2009; van Rijn 2004). It should be noted that with the membranes used, fluxes can be 20 times higher than industrial fluxes currently used and for longer periods of time.

When assuming that the liquid close to the wall will form the permeate in a filtration experiment, the resulting concentrations in permeate and retentate can be calculated from the ratio between cross-flow velocity and permeate

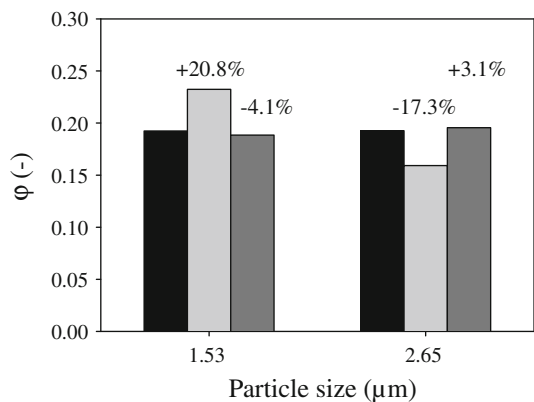


**Fig. 10** Calculated volume fraction in the bulk (black), the permeate (light grey) and the retentate (dark grey) for two different particles’ diameters. Velocity is 20.8 m/s,  $\varphi_S/\varphi_{tot}$  is 0.50 and  $\varphi_{tot}$  is 0.38

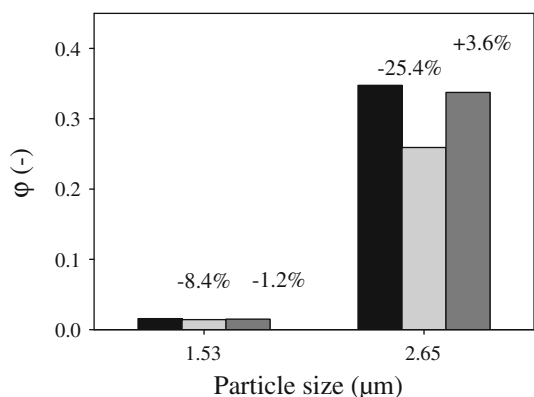


**Fig. 11** Calculated volume fraction in the bulk (black), the permeate (light grey) and the retentate (dark grey) for 1.53 μm particles. Velocity is 20.8 m/s,  $\varphi_S/\varphi_{tot}$  is 0.04 and  $\varphi_{tot}$  is 0.38

flux, as shown in Fig. 10 for a total concentration of 0.38, and equal fractions of small and large particles. The concentration of small particles increases with 20.8 %, while the concentration of large particles decreases with 17.3 %.

The selectivity ( $\alpha(-)$ ) of this process is defined in Eq. 17, and is 1.47 for this specific example.

$$\alpha = \frac{\varphi_{S,p}}{\varphi_{L,p}} \times \frac{\varphi_{L,b}}{\varphi_{S,b}} \tag{17}$$

where  $\varphi_{S,p}$ ,  $\varphi_{L,p}$  are the solid volume fractions of the small particles in the permeate (–) and the large ones, respectively, and  $\varphi_{L,b}$ ,  $\varphi_{S,b}$  are the solid volume fractions of the large particles in the bulk (–) and of the small ones, respectively.

At low relative solid volume fraction of small particles (0.04) and a concentration of 38 %, both concentrations of particles decrease in the permeate (Fig. 11), which may lead to options for overall concentration of particles. The concentration of the large and small particles decreases with 8.4 and 25.4 %, respectively, giving a selectivity of 1.25.

### 3.3 Proof of principle through membrane microfiltration

The measured and predicted effects in microchannels are now evaluated for application in (micro)filtration. A concentrated emulsion of 0.36 volume fraction and equal fractions of 2.4 and 5.1 μm ( $d_L$  is  $2.1 \cdot d_S$ ) droplets was filtered in a cross-flow membrane set-up ( $\varphi_S/\varphi_{tot}$  is 0.50). A non-porous entrance section of 34.5 cm was installed before the membrane (metallic sieve). The height of the channel was 200 μm, the cross-flow velocity was 0.59 m/s, and the transmembrane flux was  $1.0 \times 10^{-5}$  m/s. The velocity is chosen much higher than applied in the CSLM, to decrease the time needed to collect a reasonable amount of sample from the set-up. The set-up needs to be operated at the indicated flux, and to prevent droplet accumulation the velocity needs to be chosen as indicated. The channel height was 200 μm to prevent severe pressure drops, and the membrane had pores of 20 μm, being 3.7 times larger than the diameter of the large droplets.

Even though conditions are slightly different from the CSLM experiments, inertial lift and Brownian diffusion can still be neglected, i.e. maximum  $Re_p$  is 0.01 (Eq. 15) and  $Pe_{Brown}$  is smaller than  $10^{-5}$  (Eq. 8). When assuming monodisperse samples, the time scale for convection is also longer than the time scale for shear-induced diffusion ( $Pe_{shear} < 1$ , Eq. 11), although this requirement is not met for the 2.4 μm droplets in the second experiment with 0.27 oil volume fraction.

In Fig. 12, the droplet size distribution (volume%) of the bulk and the permeate are shown (there was no change in size distribution as function of time in any of the membrane experiments, indicating that no droplet accumulation takes place). A clear shift towards smaller droplets in the permeate is seen. The actual increase in small droplets is around 30 % and the decrease of large droplets in the permeate is 29 %, which leads to a change in ratio small to large of 1.78 in the permeate (in the bulk this ratio is 1.03). The values found here are slightly better than found in the CSLM experiment (selectivity 1.47). This is very likely related to an additional skimming effect of large and small droplets above the pores of the membrane, which has also been observed for less concentrated suspensions in earlier work with the same membranes/sieves (van Dintner et al. 2011). The experiment here clearly shows that ‘pre-fractionation’ in the non-porous entrance section was achieved, as separation of such concentrated emulsions of 36 % would otherwise not be possible.

A second experiment was performed to maximise the effects and for this an emulsion of 0.27 volume fraction and droplets of 2.4 and 5.4 μm ( $d_L$  is  $2.2 \cdot d_S$ ) were filtered in a cross-flow membrane set-up ( $\varphi_S/\varphi_{tot}$  is 0.89). The transmembrane flux was  $9.4 \times 10^{-6}$  m/s. The other

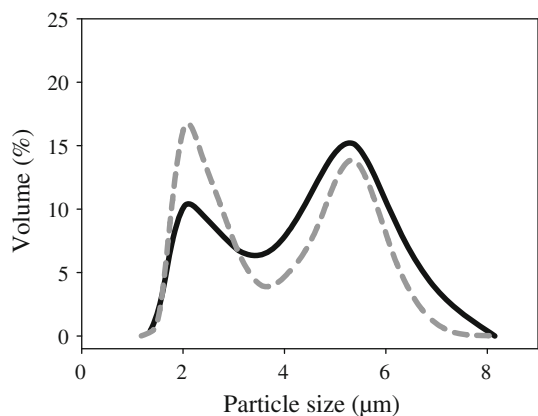


**Fig. 12** Droplet size distribution for bulk (*solid line*) and the permeate (*dashed line*). Bulk consists of 2.4 and 5.1  $\mu\text{m}$  droplets.  $\phi_{\text{tot}}$  is 0.36,  $\phi_S/\phi_{\text{tot}}$  is 0.50,  $v$  is 0.59 m/s, flux is  $1.0 \times 10^{-5}$  m/s

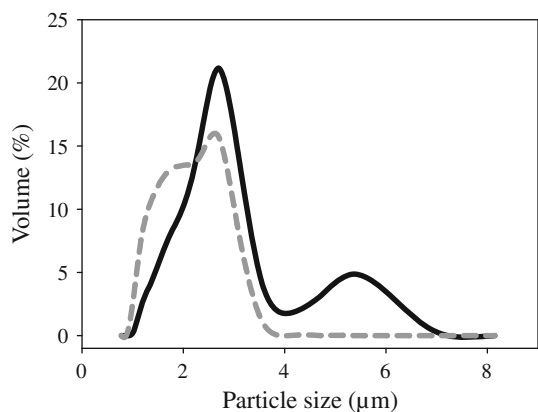


**Fig. 13** Droplet size distribution for bulk (*solid line*) and the permeate (*dashed line*). Bulk consists of 2.4 and 5.4  $\mu\text{m}$  droplets.  $\phi_{\text{tot}}$  is 0.27,  $\phi_S/\phi_{\text{tot}}$  is 0.89,  $v$  is 0.59 m/s, flux is  $9.4 \times 10^{-6}$  m/s

conditions were as described before. In Fig. 13, the droplet size distribution (volume percentage) of the bulk and the permeate are shown, and in this case droplets  $>4 \mu\text{m}$  did

not end up in the permeate, and the number of small droplets in the permeate increased with 12 %. Since the flux is constant in time, it is clear that the observed effects can be attributed to droplet migration and not to droplet accumulation, which may lead to a very sharp size segregation as indicated in Fig. 13.

The difference between Figs. 12 and 13 is probably caused by the difference in  $\phi_S/\phi_{\text{tot}}$  ratio. When the ratio is close to 0.50 (Fig. 12), large droplets migrate to the middle and small ones are present in higher concentrations at the walls; segregation is taking place. However, migration is not strong and therefore the selectivity of the process is not very high. When the fraction of small droplets is increased to  $\phi_S/\phi_{\text{tot}}$  is 0.89 (Fig. 13), the large droplets migrate sufficiently away from the wall. The small droplets are not really migrating; a similar trend was also observed in the article of Lyon and Leal (1998b). However, more importantly, the increase in small droplet concentration in the permeate may only be 12 %, but the permeate is free of large droplets, leading to very high selectivity. This striking example signifies the importance of knowledge on droplet migration for design of membrane fractionation processes.

The observed effects are a result of the droplet migration occurring in the non-porous entrance section of the channel. If this non-porous entrance section is reduced, the migration of the droplets and therewith the selectivity of the process strongly reduces. Figure 14a shows the results for an emulsion filtered with 34.5 cm non-porous entrance length, while Fig. 14b shows the results for an emulsion filtered with 6.0 cm non-porous entrance length; for the same process conditions.

In summary, the experimental results show that micro-filtration can benefit from flow-induced fractionation, when operated under appropriate process conditions. The major advantage of such approach is that separation can be

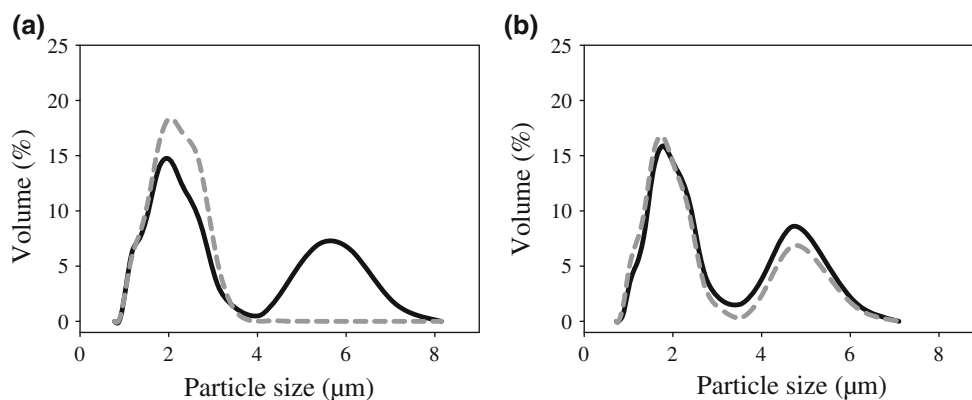


**Fig. 14 a** Droplet size distribution for bulk (*solid line*) and the permeate (*dashed line*). Bulk consists of 2.0 and 5.6  $\mu\text{m}$  droplets.  $\phi_{\text{tot}}$  is 0.35,  $\phi_S/\phi_{\text{tot}}$  is 0.81,  $v$  is 0.3 m/s, flux is  $4.8 \times 10^{-6}$  m/s. Non-porous entrance length is 34.5 cm. **b** Droplet size distribution for bulk

(*solid line*) and the permeate (*dashed line*). Bulk consists of 2.1 and 5.5  $\mu\text{m}$  droplets.  $\phi_{\text{tot}}$  is 0.35,  $\phi_S/\phi_{\text{tot}}$  is 0.79,  $v$  is 0.3 m/s, flux is  $4.8 \times 10^{-6}$  m/s. Non-porous entrance length is 6.0 cm

achieved while avoiding process deterioration due to membrane fouling. Since the pore size is no longer the determining factor for separation, the pore size can be chosen at will, while allowing high fluxes up to  $1.7 \times 10^3 \text{ L h}^{-1} \text{ m}^{-2} \text{ bar}^{-1}$  and no flux reduction in time. Industrial fluxes of this order of magnitude can currently only be maintained for very short periods of time (Moraru and Ulrich Schrader 2009; van Rijn 2004). Operation was at slightly higher transmembrane pressures than predicted in Sect. 3.2 and therefore the flux is slightly lower than mentioned in Sect. 3.2.

The shear-induced diffusion mechanism can be most efficiently used at high concentrations, i.e., the processes may be relatively compact, while the conditions are very mild (laminar flow). The CSLM measurements, while not in quantitative agreement with the filtration results, show that shear-induced migration in these concentrated emulsions is probably the underlying mechanism.

It is expected that fractionation can be further optimised when the permeate flux and channel height of the module are decreased, thereby increasing shear-induced diffusion and making optimal use of the separation close to the wall. This may be a challenge for membrane module manufacturers, but obviously the rewards can be great.

## 4 Conclusions

The new approach presented here for microfiltration uses shear-induced migration of micron sized particles in microchannels to facilitate fractionation. Particles migrated well within the first 0.1 m of the rectangular microchannel with nonporous walls used in CSLM analysis. The concentration profiles were measured as function of the particle volume fractions (profiles are more pronounced at higher concentration) and ratio between large and small particles. When the solid volume fractions of small and large particles (1.53 and 2.65  $\mu\text{m}$  in diameter, respectively) were equal at a total concentration of around 40 %, large particles migrated to the middle of the channel, while smaller ones moved closer to the wall.

This was experimentally verified for emulsions of 36 and 27 %, leading to significant selectivity, and in one case even exclusion of large droplets from the permeate. The processes were carried out at fluxes of up to  $1.7 \times 10^3 \text{ L h}^{-1} \text{ m}^{-2} \text{ bar}^{-1}$  and no flux reduction took place in time, indicating no droplet deposition during operation. To make optimal use of droplet migration, the membrane module should start with a microchannel with nonporous walls where droplets have time to migrate, followed by a separation area where the permeate is collected, and this should be feasible to implement in practice.

**Acknowledgments** The authors would like to thank J.C.P. Stiefel-hagen and P. Helfferich of the Soft Condensed Matter Group at the University of Utrecht for particle synthesis and technical support with the CSLM. Support for this work was provided by the Institute of Sustainable Process Technology, Pentair X-flow, FrieslandCampina and Royal Cosun. Special thanks to the people of the SHIFT team and the mechanical workshop of Wageningen University.

## Appendix

$$J = \frac{\Delta P}{\eta R_m} \quad (18)$$

where  $J$  is the permeate flux ( $\text{m}^3 \text{ m}^{-2} \text{ s}^{-1}$ ),  $\Delta P$  is the transmembrane pressure (Pa),  $\eta$  is the viscosity (Pa s) and  $R_m$  the membrane resistance ( $\text{m}^{-1}$ ) (Table 2)

**Table 2** Summary of process conditions and membrane characteristics to predict fractionation in a membrane microfiltration experiment

Fluid velocity in channel	$5.9 \times 10^{-1}$	m/s
Channel width	$1.6 \times 10^{-2}$	m
Channel height	$2.0 \times 10^{-4}$	m
Volumetric flow rate through channel	$1.9 \times 10^{-4}$	$\text{m}^3/\text{s}$
Volumetric permeate flow	$1.4 \times 10^{-9}$	$\text{m}^3/\text{s}$
Thickness fluid layer for permeate	$1.5 \times 10^{-7}$	m
Membrane area	$1.4 \times 10^{-4}$	$\text{m}^2$
Permeate flux	$1.0 \times 10^{-5}$	$\text{m}^3 \text{ m}^{-2} \text{ s}^{-1}$
Viscosity	$2.5 \times 10^{-3}$	Pa s
Membrane resistance	$3.3 \times 10^{-9}$	$\text{m}^{-1}$
Transmembrane pressure	$8.3 \times 10^{-4}$	bar
Permeate flux	$4.4 \times 10^4$	$\text{L h}^{-1} \text{ m}^{-2} \text{ bar}^{-1}$

## References

- Abbasi M, Sebzari MR, Salahi A, Mirza B (2011) Modelling of membrane fouling and flux decline in microfiltration of oily wastewater using ceramic membranes. *Chem Eng Commun* 199(1):78–93. doi:10.1080/00986445.2011.570391
- Abbott JR, Tetlow N, Graham AL, Altobelli SA, Fukushima E, Mondy LA, Stephens TS (1991) Experimental-observations of particle migration in concentrated suspensions—Couette-flow. *J Rheol* 35(5):773–795. doi:10.1122/1.550157
- Ackerson BJ (1991) Shear induced order in equilibrium colloidal liquids. *Phys A* 174(1):15–30. doi:10.1103/PhysRevLett.61.1033
- Acrivós A, Mauri R, Fan X (1993) Shear-induced resuspension in a couette device. *Int J Multiph Flow* 19(5):797–802. doi:10.1016/0301-9322(93)90043-T
- Asmolov ES (1999) The inertial lift on a spherical particle in a plane Poiseuille flow at large channel Reynolds number. *J Fluid Mech* 381:63–87. doi:10.1017/S0022112098003474
- Belfort G (1989) Fluid mechanics in membrane filtration: recent developments. *J Membr Sci* 40(2):123–147. doi:10.1016/0376-7388(89)89001-5

- Belfort G, Davis RH, Zydney AL (1994) The behavior of suspensions and macromolecular solutions in cross-flow microfiltration. *J Membr Sci* 96(1–2):1–58. doi:[10.1016/0376-7388\(94\)00119-7](https://doi.org/10.1016/0376-7388(94)00119-7)
- Bhagat AAS, Kuntaegowdanahalli SS, Papautsky I (2009) Inertial microfluidics for continuous particle filtration and extraction. *Microfluid Nanofluid* 7(2):217–226. doi:[10.1007/s10404-008-0377-2](https://doi.org/10.1007/s10404-008-0377-2)
- Bhagat A, Bow H, Hou H, Tan S, Han J, Lim C (2010) Microfluidics for cell separation. *Med Biol Eng Comput* 48(10):999–1014. doi:[10.1007/s11517-010-0611-4](https://doi.org/10.1007/s11517-010-0611-4)
- Bosma G, Pathmamanoharan C, de Hoog EHA, Kegel WK, van Blaaderen A, Lekkerkerker HNW (2002) Preparation of monodisperse, fluorescent PMMA–latex colloids by dispersion polymerization. *J Colloid Interface Sci* 245(2):292–300. doi:[10.1006/jcis.2001.7986](https://doi.org/10.1006/jcis.2001.7986)
- Breedveld V, van den Ende D, Jongschaap R, Mellema J (2001) Shear-induced diffusion and rheology of noncolloidal suspensions: time scales and particle displacements. *J Chem Phys* 114(13):5923–5936. doi:[10.1063/1.1355315](https://doi.org/10.1063/1.1355315)
- Chow AW, Sinton SW, Iwamiya JH, Stephens TS (1994) Shear-induced particle migration in couette and parallel-plate viscometers—Nmr imaging and stress measurements. *Phys Fluids* 6(8):2561–2576. doi:[10.1063/1.868147](https://doi.org/10.1063/1.868147)
- Di Carlo D (2009) Inertial microfluidics. *Lab Chip* 9(21):3038–3046. doi:[10.1039/B912547G](https://doi.org/10.1039/B912547G)
- Eckstein EC, Bailey DG, Shapiro AH (1977) Self-diffusion of particles in shear-flow of a suspension. *J Fluid Mech* 79(1):191–208. doi:[10.1017/S0022112077000111](https://doi.org/10.1017/S0022112077000111)
- El Rayess Y, Albasi C, Bacchin P, Taillandier P, Raynal J, Mietton-Peuchot M, Devatine A (2011) Cross-flow microfiltration applied to oenology: a review. *J Membr Sci* 382(1–2):1–19. doi:[10.1016/j.memsci.2011.08.008](https://doi.org/10.1016/j.memsci.2011.08.008)
- Eloot S, De Bisschop F, Verdonck P (2004) Experimental evaluation of the migration of spherical particles in three-dimensional Poiseuille flow. *Phys Fluids* 16(7):2282–2293. doi:[10.1063/1.1723465](https://doi.org/10.1063/1.1723465)
- Field RW, Wu D, Howell JA, Gupta BB (1995) Critical flux concept for microfiltration fouling. *J Membr Sci* 100(3):259–272. doi:[10.1016/0376-7388\(94\)00265-Z](https://doi.org/10.1016/0376-7388(94)00265-Z)
- Fillaudeau L, Carrere H (2002) Yeast cells, beer composition and mean pore diameter impacts on fouling and retention during cross-flow filtration of beer with ceramic membranes. *J Membr Sci* 196(1):39–57. doi:[10.1016/S0376-7388\(01\)00568-3](https://doi.org/10.1016/S0376-7388(01)00568-3)
- Graham AL, Altobelli SA, Fukushima E, Mondy LA, Stephens TS (1991) Nmr imaging of shear-induced diffusion and structure in concentrated suspensions undergoing couette-flow. *J Rheol* 35(1):191–201. doi:[10.1122/1.550227](https://doi.org/10.1122/1.550227)
- Kromkamp J (2005) Particle separation and fractionation by microfiltration. Wageningen University, Wageningen
- Kromkamp J, Faber F, Schroen K, Boom R (2006) Effects of particle size segregation on crossflow microfiltration performance: control mechanism for concentration polarisation and particle fractionation. *J Membr Sci* 268(2):189–197. doi:[10.1016/j.memsci.2005.06.012](https://doi.org/10.1016/j.memsci.2005.06.012)
- Leighton D, Acrivos A (1987a) Measurement of shear-induced self-diffusion in concentrated suspensions of spheres. *J Fluid Mech* 177:109–131. doi:[10.1017/S0022112087000880](https://doi.org/10.1017/S0022112087000880)
- Leighton D, Acrivos A (1987b) The shear-induced migration of particles in concentrated suspensions. *J Fluid Mech* 181:415–439. doi:[10.1017/S0022112087002155](https://doi.org/10.1017/S0022112087002155)
- Lenhof A, Laurell T (2010) Continuous separation of cells and particles in microfluidic systems. *Chem Soc Rev* 39(3):1203–1217. doi:[10.1039/B915999C](https://doi.org/10.1039/B915999C)
- Lyon MK, Leal LG (1998a) An experimental study of the motion of concentrated suspensions in two-dimensional channel flow. Part 1. Monodisperse systems. *J Fluid Mech* 363:25–56. doi:[10.1017/S0022112098008817](https://doi.org/10.1017/S0022112098008817)
- Lyon MK, Leal LG (1998b) An experimental study of the motion of concentrated suspensions in two-dimensional channel flow. Part 2. Bidisperse systems. *J Fluid Mech* 363:57–77. doi:[10.1017/S0022112098008829](https://doi.org/10.1017/S0022112098008829)
- McLaughlin JB (1993) The lift on a small sphere in wall-bounded linear shear flows. *J Fluid Mech* 246:249–265. doi:[10.1017/S0022112093000114](https://doi.org/10.1017/S0022112093000114)
- Moraru C, Ulrich Schrader E (2009) Applications of membrane separation in the brewing industry. In: Pabby AK, Rizvi SSH, Sastre AM (eds) *Handbook of Membrane Separations*. CRC Press, Taylor & Francis, pp 553–579. doi:[10.1201/9781420009484.ch20](https://doi.org/10.1201/9781420009484.ch20)
- Nandi BK, Uppaluri R, Purkait MK (2011) Identification of optimal membrane morphological parameters during microfiltration of mosambi juice using low cost ceramic membranes. *LWT Food Sci Technol* 44(1):214–223. doi:[10.1016/j.lwt.2010.06.026](https://doi.org/10.1016/j.lwt.2010.06.026)
- Nott PR, Brady JF (1994) Pressure-driven flow of suspensions—Simulation and theory. *J Fluid Mech* 275:157–199. doi:[10.1017/S0022112094002326](https://doi.org/10.1017/S0022112094002326)
- Pamme N (2007) Continuous flow separations in microfluidic devices. *Lab Chip* 7(12):1644–1659. doi:[10.1039/B712784G](https://doi.org/10.1039/B712784G)
- Park J-S, Song S-H, Jung H-I (2009) Continuous focusing of microparticles using inertial lift force and vorticity via multi-orifice microfluidic channels. *Lab Chip* 9(7):939–948. doi:[10.1039/B813952K](https://doi.org/10.1039/B813952K)
- Phillips RJ, Armstrong RC, Brown RA, Graham AL, Abbott JR (1992) A constitutive equation for concentrated suspensions that accounts for shear-induced particle migration. *Phys Fluids A Fluid Dyn* 4(1):30–40. doi:[10.1063/1.858498](https://doi.org/10.1063/1.858498)
- Piron E, Rene F, Latrille E (1995) A cross-flow microfiltration model-based on integration of the mass-transport equation. *J Membr Sci* 108(1–2):57–70. doi:[10.1016/0376-7388\(95\)00141-4](https://doi.org/10.1016/0376-7388(95)00141-4)
- Rezaei H, Ashtiani FZ, Fouladitajar A (2011) Effects of operating parameters on fouling mechanism and membrane flux in cross-flow microfiltration of whey. *Desalination* 274(1–3):262–271. doi:[10.1016/j.desal.2011.02.015](https://doi.org/10.1016/j.desal.2011.02.015)
- Semwogerere D, Weeks ER (2008) Shear-induced particle migration in binary colloidal suspensions. *Phys Fluids* 20(4):0433061–0433067. doi:[10.1063/1.2907378](https://doi.org/10.1063/1.2907378)
- Semwogerere D, Morris JF, Weeks ER (2007) Development of particle migration in pressure-driven flow of a Brownian suspension. *J Fluid Mech* 581: 437–451. doi:[10.1017/S0022112007006088](https://doi.org/10.1017/S0022112007006088)
- Shah RK, London AL (1978) *Laminar flow forced convection in ducts: a source book for compact heat exchanger analytical data, vol 1. Advances in Heat Transfer: Supplement*. Academic Press, New York
- Shakib-Manesh A, Raiskinmaki P, Koponen A, Kataja M, Timonen J (2002) Shear stress in a Couette flow of liquid-particle suspensions. *J Stat Phys* 107(1–2):67–84. doi:[10.1023/A:1014598201975](https://doi.org/10.1023/A:1014598201975)
- Strathmann H (2001) Membrane separation processes: current relevance and future opportunities. *AIChE J* 47(5):1077–1087. doi:[10.1002/aic.690470514](https://doi.org/10.1002/aic.690470514)
- Tan KW (2003) Experimental investigation of shear-induced particle migration in steady-state isothermal extrusion. *J Soc Rheol* 31(3):165. doi:[10.1678/rheology.31.165](https://doi.org/10.1678/rheology.31.165)
- Tetlow N, Graham AL, Ingber MS, Subia SR, Mondy LA, Altobelli SA (1998) Particle migration in a couette apparatus: experiment and modeling. *J Rheol* 42(2):307–327. doi:[10.1122/1.550954](https://doi.org/10.1122/1.550954)
- van Dinter AMC, Schroën CGPH, Boom RM (2009) Design of Microsieves and Microsieve Processes for Suspension Fractionation. In: Mueller A, Guieysse B, Sarkar A (eds) *New Membranes and Advanced Materials for Wastewater Treatment, vol 1022. ACS Symposium Series*. American Chemical Society, pp 137–149. doi:[10.1021/bk-2009-1022.ch009](https://doi.org/10.1021/bk-2009-1022.ch009)

- van Dintter AMC, Schroën CGPH, Boom RM (2011) High-flux membrane separation using fluid skimming dominated convective fluid flow. *J Membr Sci* 371(1–2):20–27. doi:[10.1016/j.memsci.2011.01.013](https://doi.org/10.1016/j.memsci.2011.01.013)
- van Rijn CJM (2004) Nano and micro engineered membrane technology. Membrane science and technology series, vol 10, 1st edn. Elsevier, Amsterdam; Boston. doi:[10.1016/S0927-5193\(04\)80017-2](https://doi.org/10.1016/S0927-5193(04)80017-2)
- Vollebregt HM, van der Sman RGM, Boom RM (2010) Suspension flow modelling in particle migration and microfiltration. *Soft Matter* 6(24):6052–6064. doi:[10.1039/C0SM00217H](https://doi.org/10.1039/C0SM00217H)
- Weigl BH, Yager P (1999) Microfluidic Diffusion-Based Separation and Detection. *Science* 283(5400):346–347. doi:[10.1126/science.283.5400.346](https://doi.org/10.1126/science.283.5400.346)
- Whitesides GM (2006) The origins and the future of microfluidics. *Nature* 442(7101):368–373. doi:[10.1038/nature05058](https://doi.org/10.1038/nature05058)
- Yu ZS, Shao XM, Tanner R (2007) Dynamic simulation of shear-induced particle migration in a two-dimensional circular couette device. *Chin J Chem Eng* 15(3):333–338. doi:[10.1016/S1004-9541\(07\)60089-5](https://doi.org/10.1016/S1004-9541(07)60089-5)
- Zeng L, Balanchandar S, Fischer P (2005) Wall-induced forces on a rigid sphere at finite Reynolds number. *J Fluid Mech* 536:1–25. doi:[10.1017/S0022112005004738](https://doi.org/10.1017/S0022112005004738)
- Zhao C, Cheng X (2011) Microfluidic separation of viruses from blood cells based on intrinsic transport processes. *Biomicrofluidics* 5(3):032004. doi:[10.1063/1.3609262](https://doi.org/10.1063/1.3609262)